Iraqi Journal of Scientific and Industrial Research
Volume 3, Issue (3), July-September 2024, pp. 17-20

Temporally and Spatially Localized Phase Transformations in Ferrous Alloys by Rapid Laser Irradiation

Sameer A. Mohammed, Enad S. Kadhim, Rasool M. Alwan

Department of Mechanical Engineering, College of Engineering, University of Najaf, Najaf, IRAQ

Abstract

In this study, the temporally and spatially localized phase transformations in ferrous alloys were investigated. These transformations were temporally restricted by rapid irradiation with laser pulses and quenching by liquid nitrogen jet flow. The spatial localization of these phase transformations was carried out by placing the sample of ferrous alloy between two thermal and electrical insulators to prevent any heat or charge flow towards the surrounding. The optical microscopy was used for introducing the microstructures of the ferrous alloy samples. It was shown that the temporal and spatial localization can enhance the eutectic and eutectoid positions on the iron-carbon phase diagrams to which the ferrous alloy are classified.

Keywords: Phase transformation; Ferrous alloys; Cast iron; Heat treatment

Received: 12 February 2024; **Revised:** 15 May 2024; **Accepted:** 22 May 2024; **Published:** 1 July 2024

1. Introduction

Ferrous alloys components have been produced from the liquid state for many centuries with mass production of steel commencing in the late nineteenth century. Molten steel was traditionally cast into standing molds, but continuous casting was developed in the 1950s which enabled the production of huge tonnages of steel. Most of the world's steel production is now obtained through this casting route. Following casting, as-cast slabs are thermal and mechanical processed to the desired final shape [1]. In the last few decades, however, near-net-shape casting processes have been developed that are capable of producing near-final-shape products directly from liquid with secondary processing such as hot rolling reduced to an absolute minimum [2]. On a reduced scale, there are various types of novel iron alloys produced in the amorphous, nanocrystalline, and intermetallic form. These materials are either manufactured by conventional casting or by rapid solidification processing, spray deposition, mechanical attrition, and sintering or physical and chemical vapor deposition, etc. Iron alloys produced by these more exotic techniques are generally restricted to specific applications [3]. Recent advances in additive manufacturing technologies such as 3D printing have enabled conventional and more novel iron alloys to be directly net-shape fabricated into complex final shapes and intricate components [4-6].

Ferrous alloys, especially steels, are the most important construction materials due to their high mechanical properties, abundance, and reasonable prices. Steel-based composites are of little importance when improvement in mechanical properties such as tensile strength is concerned [7]. However, in some cases, density reduction, improved wear resistance and enhanced high-temperature properties have become the major motivation for the processing of this group of composite materials. Zirconia-reinforced steel has been produced by infiltration method [8]. Lower friction coefficient and better wear behavior of the composite has been reported. Similar effects are reported [9] for the addition of Al_2O_3 particulates to steels.

In general, cast irons are a class of ferrous alloys with carbon contents above 2.14 wt.%; in practice, however, most cast irons contain between 3.0 and 4.5 wt.% C and, in addition, other alloying elements. A reexamination of the iron–iron carbide phase diagram (Fig. 1) reveals that alloys within this composition range become completely liquid at temperatures

between approximately 1150 and 1300°C, which is considerably lower than for steels [1,2]. Thus, they are easily melted and amenable to casting. Furthermore, some cast irons are very brittle, and casting is the most convenient fabrication technique [3].

Cementite (Fe_3C) is a metastable compound, and under some circumstances it can be made to dissociate or decompose to form α-ferrite and graphite, according to the reaction [4]

$$Fe_3C \rightarrow 3Fe\ (\alpha) + C\ (\text{graphite}) \qquad (1)$$

Thus, the true equilibrium diagram for iron and carbon is not that presented in Fig. (1), but rather as shown in Fig. (2). The two diagrams are virtually identical on the iron-rich side (e.g., eutectic and eutectoid temperatures for the Fe–Fe_3C system are 1147 and 727°C, respectively, as compared to 1153 and 740°C for Fe–C); however, figure (2) extends to 100 wt% C such that graphite is the carbon-rich phase, instead of cementite at 6.7 wt% C (Fig. 1) [4,5]

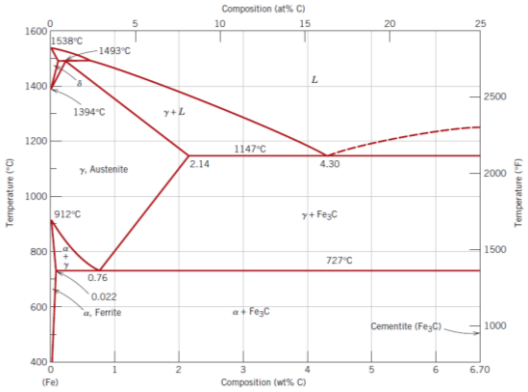

Fig. (1) The iron–iron carbide phase diagram [5]

This tendency to form graphite is regulated by the composition and rate of cooling. Graphite formation is promoted by the presence of silicon in concentrations greater than about 1 wt%. Also, slower cooling rates during solidification favor graphitization (the formation of graphite) [6]. For most cast irons, the carbon exists as graphite, and both microstructure and mechanical behavior depend on composition and heat treatment. The most common cast iron types are gray, nodular, white, malleable, and compacted graphite [7-10].

The carbon and silicon contents of gray cast irons vary between 2.5 and 4.0 wt.% and 1.0 and 3.0 wt.%, respectively. For most of these cast irons, the graphite exists in the form of flakes (similar to corn flakes), which are normally surrounded by an α-ferrite or pearlite matrix; the microstructure of a typical gray iron is shown in Fig. (3a). Because of these graphite flakes, a fractured surface takes on a gray appearance, hence its name.

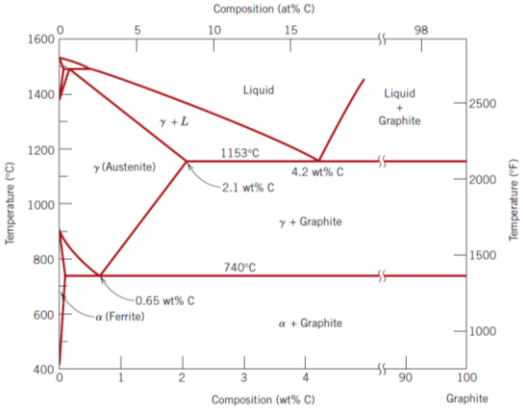

Fig. (2) The true equilibrium iron–carbon phase diagram with graphite instead of cementite as a stable phase [5]

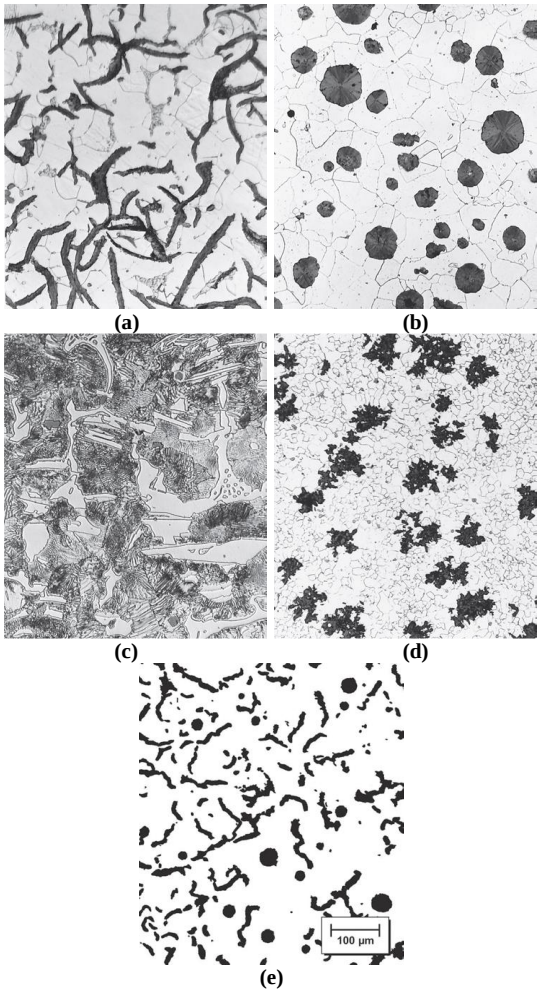

Fig. (3) Optical photomicrographs of various cast irons. (*a*) Gray iron: the dark graphite flakes are embedded in an *α*-ferrite matrix. 500μ. (*b*) Nodular (ductile) iron: the dark graphite nodules are surrounded by an *α*-ferrite matrix. 200μ. (*c*) White iron: the light cementite regions are surrounded by pearlite, which has the ferrite–cementite layered structure. 400μ. (*d*) Malleable iron: dark graphite rosettes (temper carbon) in an *α*-ferrite matrix. 150μ. (*e*) Compacted graphite iron: dark graphite wormlike particles are embedded within an *α*-ferrite matrix. 100μ [11]

Mechanically, gray iron is comparatively weak and brittle in tension as a consequence of its microstructure; the tips of the graphite flakes are sharp and pointed and may serve as points of stress concentration when an external tensile stress is applied. Strength and ductility are much higher under compressive loads. Gray irons do have some desirable characteristics and are utilized extensively. They are very effective in damping vibrational energy; this is represented in Fig. (4), which compares the relative damping capacities of steel and gray iron. Base structures for machines and heavy equipment that are exposed to vibrations are frequently constructed of this material. In addition, gray irons exhibit a high resistance to wear. Furthermore, in the molten state they have a high fluidity at casting temperature, which permits casting pieces that have intricate shapes; also, casting shrinkage is low. Finally, and perhaps most important, gray cast irons are among the least expensive of all metallic materials.

Gray irons having microstructures different from that shown in Fig. (3a) may be generated by adjustment of composition and/or by using an appropriate treatment. For example, lowering the silicon content or increasing the cooling rate may prevent the complete dissociation of cementite to form graphite (Eq. 1) [12-14]. Under these circumstances the microstructure consists of graphite flakes embedded in a pearlite matrix. Figure (5) compares schematically the several cast iron microstructures obtained by varying the composition and heat treatment [15,16].

Adding a small amount of magnesium and/or cerium to the gray iron before casting produces a distinctly different microstructure and set of mechanical properties [17-19]. Graphite still forms, but as nodules or spherelike particles instead of flakes. The resulting alloy is called ductile or nodular iron, and a typical microstructure is shown in Fig. (3b). The matrix phase surrounding these particles is either pearlite or ferrite, depending on heat treatment (Fig. 5); it is normally pearlite for an as cast piece. However, a heat treatment for several hours at about 700°C will yield a ferrite matrix as in this photomicrograph. Castings are stronger and much more ductile than gray iron. In fact, ductile iron has mechanical characteristics approaching those of steel. For example, ferritic ductile irons have tensile strengths ranging between 380 and 480 MPa (55,000 and 70,000 psi), and ductilities (as percent elongation) from 10% to 20% [20-22]. Typical applications for this material include valves, pump bodies, crankshafts, gears, and other automotive and machine components.

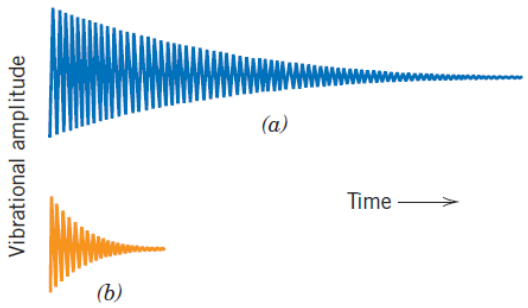

Fig. (4) Comparison of the relative vibrational damping capacities of (*a*) steel and (*b*) gray cast iron [15]

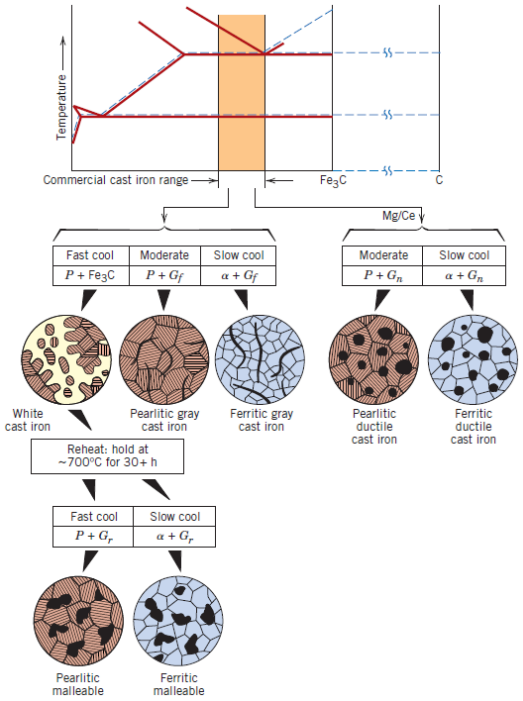

Fig. (5) From the iron–carbon phase diagram, composition ranges for commercial cast irons. Also shown are schematic microstructures that result from a variety of heat treatments. *Gf*, flake graphite; *Gr*, graphite rosettes; *Gn*, graphite nodules; *P*, pearlite; *α*, ferrite [23]

For low-silicon cast irons (containing less than 1.0 wt% Si) and rapid cooling rates, most of the carbon exists as cementite instead of graphite, as indicated in Fig. (5). A fracture surface of this alloy has a white appearance, and thus it is termed white cast iron [1]. An optical photomicrograph showing the microstructure of white iron is presented in Fig. (3c). Thick sections may have only a surface layer of white iron that was “chilled” during the casting process; gray iron forms at interior regions, which cool more slowly [24]. As a consequence of large amounts of the cementite phase, white iron is extremely hard but also very brittle, to the point of being virtually unmachinable. Its use is limited to applications that necessitate a very hard and wear-resistant surface, without a high degree of ductility—for example, as

rollers in rolling mills [25-28]. Generally, white iron is used as an intermediary in the production of yet another cast iron, malleable iron [1].

References

[1] B. Bhushan (Ed.), **"Springer Handbook of Nanotechnology"**, Springer (2004), p. 27, 151, 438.
[2] M. Ohring, **"The Materials Science of Thin Films"**, Academic Press (San Diego) (1992), p. 79, 112, 182.
[3] N. Maluf and K. Williams, **"An Introduction to Microelectromechanical Systems Engineering"**, Artech House, Inc. (2004), p. 19, 39.
[4] W.D. Callister Jr. and D.G. Rethwisch, **"Materials Science and Engineering: An Introduction"**, 8th ed., John-Wiley & Sons, Ltd. (NY, 2010), p. 399.
[5] B. Massalski (Editor-in-Chief), **"Binary Alloy Phase Diagrams"**, 2nd ed., vol. 1, ASM International (OH, 1990).
[6] M.A. Lieberman and A.J. Lichtenberg, **"Principles of Plasma Physics and Materials Processing"**, 2nd ed., Wiley (2005), p. 535, 547.
[7] P.M. Martin, **"Handbook of Thin Film Deposition Techniques"**, Elsevier (2010), p. 4.
[8] P.M. Martin, **"Introduction to Surface Engineering and Functionally Engineered Materials"**, John Wiley & Sons, Inc. (2011), pp. 262-264, p. 339.
[9] B. Shah, Deposition of Tantalum on Steel by Sputtering, MSc thesis, New Jersey Institute of Technology (2001), p. 3, 15, 30.
[10] J.C. da Conceição Lorenzzi, "Boron nitride thin films deposited by magnetron sputtering on Si_3N_4", PhD thesis, Universidade de Aveiro, Departamento de Engenharia Cerâmica e do Vidro, pp. 10-16 (2007).
[11] Figures (a) and (b) courtesy of C. H. Brady and L. C. Smith, National Bureau of Standards, Washington, DC (now the National Institute of Standards and Technology, Gaithersburg, MD). Figure (c) courtesy of Amcast Industrial Corporation. Figure (d) reprinted with permission of the Iron Castings Society, Des Plaines, IL. Figure (e) courtesy of SinterCast, Ltd.
[12] C. O'Leary, Design, Construction and Characterisation of a Variable Balance Magnetron Sputtering System, Dublin City University, Ireland, p. 15 (1999).
[13] D. Huy Trinh, Nanocrystalline Alumina-Zirconia Thin Films Grown by Magnetron Sputtering, Linköping University, Sweden, (2008) p. 1.
[14] D.R. Gibson, "Deposition of multilayer optical coatings using closed field magnetron sputtering", online article (2006).
[15] Metals Engineering Quarterly, February 1961. Copyright 1961 American Society for Metals.
[16] E.C. Paloura, J. Lagowski and H.C. Gatos, "Growth and electronic properties of thin Si_3N_4 films grown on Si in a nitrogen glow discharge", J. Appl. Phys., 69, 3995-4002 (1991).
[17] F. Ghaleb and A. Belasri, "Numerical and theoretical calculation of breakdown voltage in the electrical discharge", Radiation Effects and Defects in Solids, 1 (2012) 1-7.
[18] H. Lorentz et al., "Characterization of low temperature SiO_2 and Si_3N_4 films deposited by plasma enhanced evaporation", J. Vac. Sci. Technol. B, 9, 208-214 (1991).
[19] H.B. Nie, Thin Film Deposition and Characterization, National University of Singapore (NUS) (2014).
[20] K. Deenamma Vargheese and G. Mohan Rao, "Ion-assisted deposition of silicon nitride films using electron cyclotron resonance plasma", J. Vac. Sci. Technol. A: Vac. Surf. Films. 19(4), 1336-1340 (2001).
[21] K. Tanabashi and K. Kobayashi, "Properties of vapor deposited silicon nitride films with varying excess Si content", Jpn. J. Appl. Phys., 12, 641-646 (1973).
[22] M. Julfikar Haider, Deposition of Hard and Solid Lubricant ($TiN+MoS_x$) Coating by Closed-Field Magnetron Sputtering, PhD thesis, Dublin University, Ireland (2005), pp. 56-58, 176.
[23] W. G. Moffatt, G.W. Pearsall and J. Wulff, **"The Structure and Properties of Materials"**, Vol. I, Structure, John Wiley & Sons (NY, 1964), p. 195.
[24] K. Wasa, M. Kitabatake, H. Adachi, **"Thin Film Materials Technology: Sputtering of Compound Materials"**, William Andrew Inc., p. 139, 116, 2, 119, 72, 106, 103, 9 (2004).
[25] S.V. Deshpande et al., "Optical properties of silicon nitride films deposited by hot filament chemical vapor deposition" J. Appl. Phys., 77(12), 6534-6541 (1995).
[26] S.W. et al., "Properties of plasma-enhanced chemical-vapor-deposited a-SiN_x:H by various dilution gases", J. Appl. Phys., 76, 3645-3655 (1994).
[27] S.M. Sze, "Current transport and maximum dielectric strength of silicon nitride films", J. Appl. Phys., 38, 2951-2955 (1967).
[28] T.E. Cook Jr. et al., "Band offset measurements of the Si_3N_4/GaN (0001) interface", J. Appl. Phys., 94(6), 3949-3954 (2003).

